Investigation of Magneto-Convection Characteristics in A Sudden Expanding Channel with Convex Surface Geometry Under Thermally Developing Flow Conditions

Emrehan Gürsoy
emrehangursoy@gmail.com
Karabük University
Hayati Kadir Pazarlıoğlu
University of Stuttgart
Mehmet Gürdal
Kastamonu University
Kamil Arslan
Ankara Yıldırım Beyazıt University
Engin Gedik
Karabük University
Abdullah Dağdeviren
Karabük University

Research Article

Keywords: Sudden expansion tube, Dimpled fin, DC magnetic field, Fe3O4/H2O Ferrofluid, Performance Evaluation Criterion.

Posted Date: October 23rd, 2023

DOI: https://doi.org/10.21203/rs.3.rs-3449356/v1

Additional Declarations: No competing interests reported.

Version of Record: A version of this preprint was published at International Journal of Numerical Methods for Heat & Fluid Flow on March 25th, 2024. See the published version at https://doi.org/10.1108/HFF-11-2023-0703.

Investigation of Magneto-Convection Characteristics in A Sudden Expanding Channel with Convex Surface Geometry Under Thermally Developing Flow Conditions

Emrehan Gürsoy[a,b*], Hayati Kadir Pazarlıoğlu[c*], Mehmet Gürdal[b,d], Kamil Arslan[b,e], Engin Gedik[b,f], Abdullah Dağdeviren[a,b]

[a]Department of Energy Systems Engineering, Karabük University, Türkiye
[b]Center of Energy Applications Laboratory, Karabük University, Türkiye
[c]Institute of Aerospace Thermodynamics, University of Stuttgart, Germany
[d]Department of Mechanical Engineering, Kastamonu University, Türkiye
[e]Department of Mechanical Engineering, Ankara Yıldırım Beyazıt University, Türkiye
[f]Department of Mechanical Engineering, Karabük University, Türkiye

Abstract

The current study presents a novelty with focusing on the magnetic field effect on a sudden expansion tube with expansion ratio, total length, and pitch length of the dimpled fin is 2.5, 1500 *mm*, and 3.0, respectively. The magnetizable Fe_3O_4/H_2O Ferrofluid with different nanoparticle volumetric concentrations (φ=1.0% and 2.0%) were used as a heat transfer fluid, and magnetohydrodynamic effects were elaborately investigated in this study. The numerical analysis was conducted under laminar flow regime and the *DC* magnetic field (B_0=0.03*T*, 0.05*T*, 0.3*T*, and 0.5*T*). The present study provided a comprehensive investigation, which presented the thermo-hydraulic performance of difference dimpled fins, Fe_3O_4/H_2O Ferrofluid, and magnetic field. According to the results, dimple fins showed the best increment within heat transfer enhancement techniques. The heat transfer enhancement rate of the dimple tube and Fe_3O_4/H_2O Ferrofluid were respectively acquired as 22.62% and 5.43%-6.28% (φ=1.0% and 2.0%). When dimpled fin and Fe_3O_4/H_2O Ferrofluid were used, the increment in Performance Evaluation Criteria was calculated as 21.31% and 4.85%-9.79% (φ=1.0% and 2.0%). Although the highest average Nusselt number was obtained at B_0=0.5*T*, the highest performance evaluation criteria were detected at B_0=0.3*T* due to the friction factor showing an increment.

Keywords: Sudden expansion tube, Dimpled fin, *DC* magnetic field, Fe_3O_4/H_2O Ferrofluid, Performance Evaluation Criterion.

Nomenclature

AC	alternating current	*PEC*	performance evaluation criterion

*Corresponding Authors.
E-mail address: emrehangursoy@gmail.com (E. Gürsoy), hayati-kadir.pazarlioglu@itlr.uni-stuttgart.de (H.K. Pazarlıoğlu)

$\overrightarrow{B_0}$	Magnetic field intensity (*T*)	*P*	dimple distance (*mm*), pressure (*Pa*)
BF	base fluid	*P/d*	pitch ratio
d	dimple diameter (*mm*)	*Re*	Reynolds number
D	tube diameter (*mm*), dimension	*SET*	sudden expansion tube
DC	direct current	*ST*	smooth tube
DF	dimpled fin	*T*	temperature (*K*), Tesla
DT	dimpled tube	*THP*	thermo-hydraulic performance
$\vec{E}$	electrical field (V/m)	$\vec{V}$	velocity (*m/s*)
ER	expansion ratio	q''	heat flux (W/m^2)
f	frequency	***Greek symbols***	
ff	Darcy friction factor	φ	nanoparticle volumetric concentration (%)
$\vec{F}$	Lorentz force (*N*)	μ	dynamic viscosity (*Pa.s*), magnetic permeability (*H/m*)
FF	ferrofluid	Φ	dissipation energy (W/m^3)
H	dimple height (*mm*)	σ	electrical conductivity (*S/m*)
Ha	Hartmann number	Δ	difference
HTF	heat transfer fluid	ρ	density (kg/m^3)
$\vec{j}$	current density (A/m^2)	***Subscripts***	
k	thermal conductivity (*W/mK*)	*b*	bulk
L	longitudinal length (*mm*)	*bf*	base fluid
MF	magnetic field	*in*	inlet
MHD	magnetohydrodynamic	*nf*	nanofluid
Nu	Nusselt number	*np*	nanoparticle
NF	nanofluid	*out*	outlet
NP	nanoparticle	*w*	wall

1. Introduction

Global warming is one of the top issues that requires an urgent action. To reduce emission and leave a clean world for future generations 151 countries have taken considerable actions such as the "loss and damage" motto and net-zero emission by 2050 at the *COP26* summit, Glasgow Conference in 2021 [1, 2]. For this purpose, there has been significant increment in the scientific studies carried out on the use of renewable energy sources [3, 4] Most researchers have conducted a great deal of study on it. One of these studies is the heat exchanger, which is used in lots of industrial applications. The performance enhancement techniques for heat exchanger have been investigated employing passive [5] and active techniques [6] which are heat transfer improvement techniques.

For instance, rough surface, which includes dimpled fins (*DFs*), is one of the prominent passive techniques in the geometric improvement, and this phenomenon has been investigated by numerous researchers in the literature [7, 8]. Malapur et al. [9] conducted a computational analyses on five different dimpled tubes (*DT*). Researchers have aimed to investigate the effect of *DF* and compare it with the smooth tube (*ST*). According to the results, the heat transfer properties of *DT* override on *ST*, and the helical pattern of *DF* with a smaller pitch angle exhibits more heat transfer than other types of fins. Dagdevir [10] has numerically investigated the convective heat transfer (*h*) and pressure drop (ΔP)

behavior of the various *DF* parameters such as dimple diameter (*d*), dimple pitch length (*PL*), and dimple height (*H*). H_2O has been used as heat transfer fluid (*HTF*), and Reynolds number (*Re*) is considered as *Re*=3000. It was reported that the influence of *PL* is higher than the effect of *H* and *d* in terms of *h* and *ΔP*. Furthermore, it was found that *d*=7 *mm*, *PL*=30 *mm,* and *H*=1.0 mm present the optimum performance regarding hydrothermal behavior. A study aimed to determine the performance of *DT* has been carried out by Kaood et al. [11]. The numerical study has been examined under *Re*=3000-40000, constant heat flux of q''=40000 W/m^2 and using H_2O as *HTF*. As a result, the *DT* may enhance the thermal performance of the system up to 121.4% compared to *ST*. Another study, which focused on the effect of *DF* on thermohydraulic performance (*THP*), has been conducted by Zheng et al. [12]. Researchers firstly examined the actual applicability of the elliptical *DF* to be used as a passive method and created the tube with a reasonable error rate. According to the results, Performance Evaluation Criterion (*PEC*) has reached a maximum value as 2.4 using the elliptical *DF*.

Along with the improvement of the nano technology, *NFs* have been created with the help of nanoparticles, which size is less than 100 *nm* [13] and dispersed in conventional *HTFs* such as H_2O, ethylene glycol, oil, etc.[14, 15]. In fact, *NFs* have been examined together with *DF* in both experimental and numerical studies in the literature. Gürsoy et al. [16] theoretically analyzed the *THP* of ferrofluid (*FF*) in a sudden expansion tube (*SET*) retrofitted with *DF*. The analyses have been performed under $100 \leq Re \leq 2000$, q''=600 W/m^2, and $1.0\% \leq \varphi \leq 2.0\%$. The results show that the increment in *Re* affects *Nu* positively. It is also found that the flow geometry, which has an expansion ratio (*ER*) is 2.5 and a pitch ratio (*P/d*) is 3.0, at the *Re*=2000 and φ =2.0% case provides the highest *PEC*. Ahmad et al. [17] realized a comprehensive numerical study, which has a lot of double-*DF* and *NF* configurations. The study has provided important outcomes about *DF* and *NF* effects in thermal systems. The analyses have been conducted under *Re*=10000-13000 and q''=10 kW/m^2. Mono and hybrid *NFs* with $1.0\% \leq \varphi \leq 3.0\%$ have been used as *HTF*. The results demonstrated that *double-DFs* have enhanced the average *Nu* up to 168.2% compared to *ST*. Furthermore, it is seen that Al_2O_3-CuO/H_2O hybrid *NF* enhances the average *Nu* by 12.0% compared to Al_2O_3/H_2O.

With the addition of *NPs* to conventional *HTFs*, a few improvements are observed in the *THP*. The thermal and hydrodynamic behavior of the existing fluids might change in this way. Thus, a less increase in heat transfer coefficient and viscosity are among the results encountered by researchers [18]. To enhance thermal performance of the system, researchers have started to activate the magnetic field (*MF*) on the system as well as the *DFs*. Utilization of the *MF* is placed as one of the active heat transfer enhancement techniques [19] in the literature. Many experimental and numerical studies have been carried out on this subject, especially using Fe_3O_4 *NPs*. Recently, Gürdal et al. [20] have presented valuable studies in the literature about MagnetoHydroDynamics (*MHD*) area. A particular experimental study, in which the scope of *MHD*, has been carried out by Shahsavar et al. [21]. The researchers have utilized two active methods consisting of rotating *MF* and vibration to enhance the heat transfer rate of Fe_3O_4/H_2O *FF* flowing in a rifled tube. According to the results, vibration enhances the *PEC* up to 1.28.

Along with applying the rotating *MF*, *PEC* shows an increment of 21.32%. Halawa and Tanious [22] realized a numerical study to determine the optimum *MF* arrangement, which will provide the highest convective heat transfer rate in the rectangular channel using Fe_3O_4/H_2O *FF*. Researchers have presented detailed results about the problem. *MF* has reciprocatively been applied on the channel at four different locations and the magnets have been placed in *N-N*, *S-N*, and *S-S* orientations. While the *MF* intensity was ranged from 250 to 1000 *Gauss*, *N-N* magnet orientation was performed with the optimum results. The results indicated that the average *Nu* exhibits an increment range of 16.44%–24.46% applying the *MF* up to 1000 *Gauss*.

When the literature review is examined, it is seen that *MHD* applications are made for different flow geometries and application purposes. However, the effect of *DC MF* on the *THP* of *FF* flowing through *SET*, which is modernized with *DF*, has not been investigated so far. This determined purpose reveals the novelty of this study. Based on this situation, the flow geometry of which the best *PEC* has been obtained in the study (*ER*=2.5 and *P/d*=3.0) conducted by Gürsoy et al. [16] has been used for this investigation. It has numerically been handled in this study as the fundamental flow problem, and the effect of *MF* on the sudden expansion geometry with *FF* has been examined in detail. In the study, *Re*=1000, 1500, and 2000 have been used, and *FF* has been prepared as φ=1.0% and 2.0%. *DC MF* has been applied at z= 937.5 *mm* with the intensity of B_0=0.03, 0.05, 0.3, and 0.5*T*. The results are presented in the form of graphs and discussed in detail.

2. Geometry Description and Boundary Conditions

In this study, *MHD* convective heat transfer and flow characteristics of *FF* have been considered for the *SET* subjected to uniform and constant wall heat flux and *DC MF*. The flow chart of the problem, definitions, boundary conditions, and process stage of this analysis are given in Fig. 1. Besides, Fig. 2 shows description of the geometry and boundary conditions for investigated computational domain. The *HTF* enters the inlet tube of *SET* with D_1=8 *mm* and L_1=375 *mm* under laminar flow regime at 300 *K*. *HTF* is suddenly expanded at z=375 *mm* and starts flowing in the outlet tube with D_2=20 *mm* and L_2=1125 *mm*. Furthermore, *DC MF* has been applied at z=937.5 *mm* with the diversified intensities as B_0=0.03, 0.05, 0.3, and 0.5*T*. The affected area length by *MF* has been considered as L_M=100 *mm* electromagnet diameter used in the experimental study carried out by Tekir et al. [23]. The geometric parameters and boundary conditions of the numerical study are summarized in Table 1.

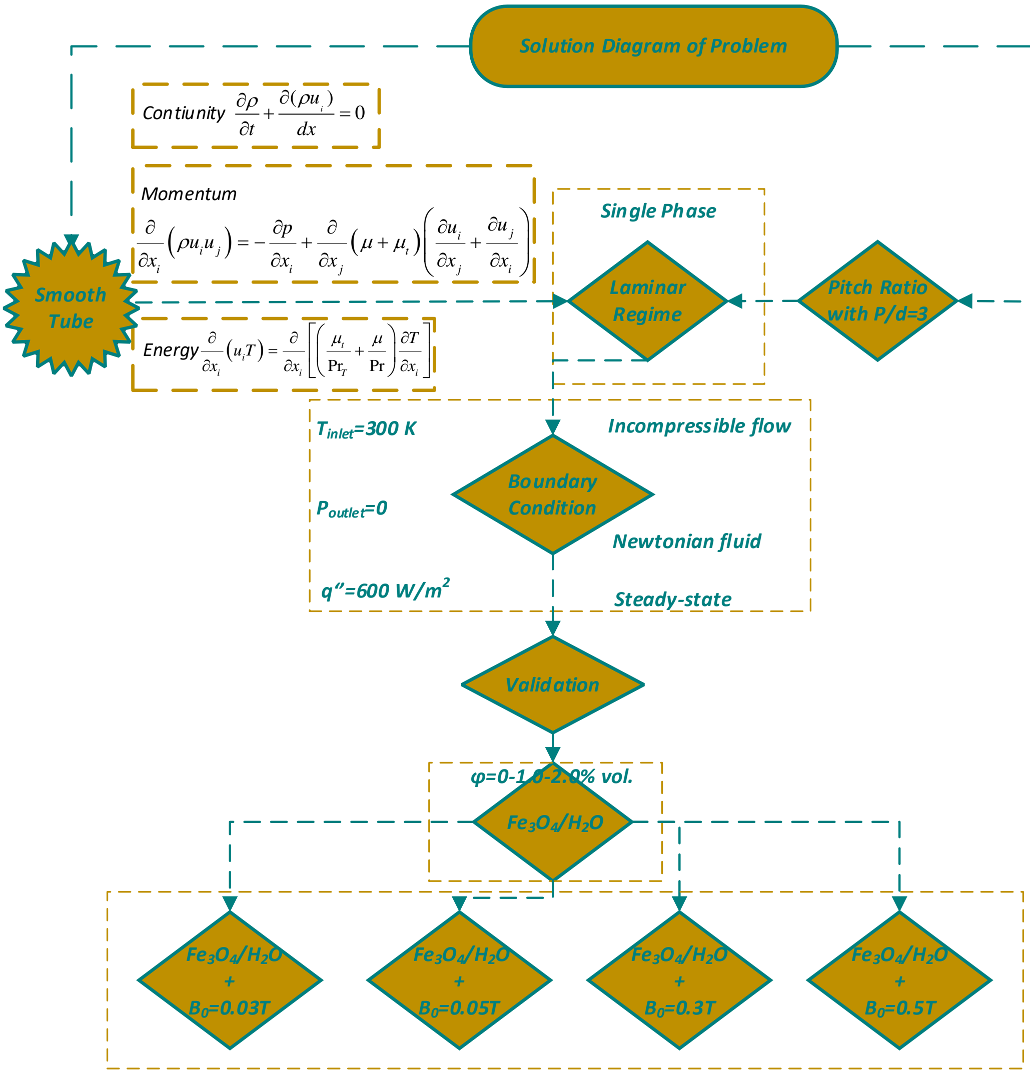

Fig. 1. Flow chart of problem solution and analysis

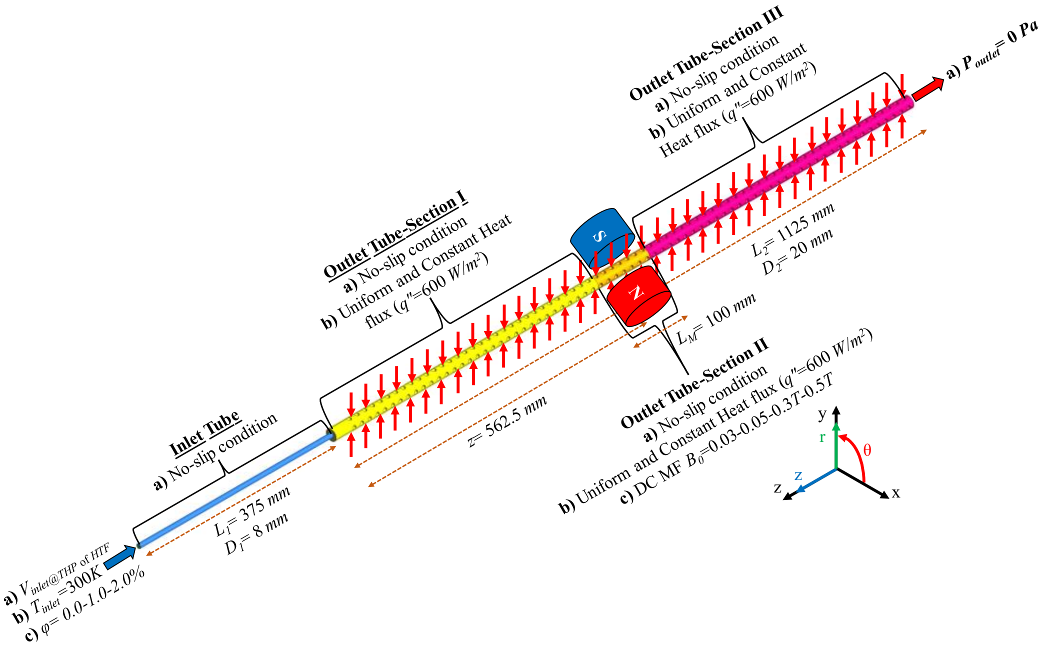

(a)

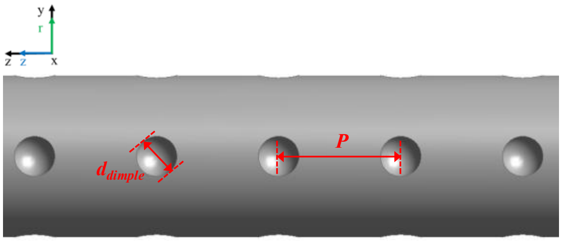

(b)

Fig. 2. Description of; (a) flow geometry and boundary conditions of the numerical study, (b) *DF* geometry.

Table 1. Geometric parameters and boundary conditions of the numerical study.

Category	Description	Parameter	Value
Geometry	Inlet tube length	L_1 (*mm*)	375
	Inlet tube diameter	D_1 (*mm*)	8
	Outlet tube length	L_2 (*mm*)	1125
	Outlet tube diameter	D_2 (*mm*)	20
	DF diameter	d_{dimple} (*mm*)	5
	Pitch length	*P* (*mm*)	15
	Location of *MF*	*z* (*mm*)	562.5
	Effect area length of *MF*	L_M (*mm*)	100
Boundary conditions	Inlet temperature	T_{inlet} (*K*)	300
	*Inlet velocity	V_{inlet} (*m/s*)	@*THP* of *HTF*
	Outlet pressure	P_{outlet} (*Pa*)	0
	Heat flux	q'' (W/m^2)	600
	FF volumetric concentration	φ (%)	0.0-1.0-2.0
	DC MF intensity	B_0 (*T*)	0.03-0.05-0.3-0.5
	Hartmann number	*Ha* (-)	0.32-0.52-3.18-5.30

* Since *Re* is constant, the inlet velocity varies according to the *THP* of the *HTF*.

3. Mathematical Modeling and Solution Procedure

In this section, mathematical formulas, thermophysical properties of *HTFs*, and solution procedure are given for solving numerical studies with the properties defined in Section 2.

3.1. Governing equations

The fluid data has been solved via Finite Volume Method. With this approach, the continuity equation is presented in Eq. (1) [24].

$$\frac{\partial \rho}{\partial t}+\frac{1}{r}\frac{\partial}{\partial r}\left(r\rho V_r\right)+\frac{1}{r}\frac{\partial\left(\rho V_\theta\right)}{\partial \theta}+\frac{\partial\left(\rho V_z\right)}{\partial z}=0 \quad (1)$$

Any change is not seen in the continuity equation with applying the *MF* [25]. The momentum equation, which analyzed the movement of *HTF* and including the Lorentz force, is given in Eq. (2-4) as component [26, 27].

r-component of Momentum equation:

$$\rho\left(V_r\frac{\partial V_r}{\partial r}+\frac{V_\theta}{r}\frac{\partial V_r}{\partial \theta}-\frac{V_\theta^2}{r}+V_z\frac{\partial V_r}{\partial z}\right)= \\ -\frac{\partial P}{\partial r}+\rho g_r+\mu\left(\frac{\partial^2 V_r}{\partial r^2}+\frac{1}{r}\frac{\partial V_r}{\partial r}-\frac{V_r}{r^2}+\frac{1}{r^2}\frac{\partial^2 V_r}{\partial \theta^2}-\frac{2}{r^2}\frac{\partial V_\theta}{\partial \theta}+\frac{\partial^2 V_r}{\partial z^2}\right)+q\left(E_0+V_r B_0\right)B_0 \tag{2}$$

θ-component of Momentum equation:

$$\rho\left(V_r\frac{\partial V_\theta}{\partial r}+\frac{V_\theta}{r}\frac{\partial V_\theta}{\partial \theta}-\frac{V_r V_\theta}{r}+V_z\frac{\partial V_\theta}{\partial z}\right)= \\ -\frac{1}{r}\frac{\partial P}{\partial \theta}+\rho g_\theta+\mu\left(\frac{\partial^2 V_\theta}{\partial r^2}+\frac{1}{r}\frac{\partial V_\theta}{\partial r}-\frac{V_\theta}{r^2}+\frac{1}{r^2}\frac{\partial^2 V_\theta}{\partial \theta^2}+\frac{2}{r^2}\frac{\partial^2 V_r}{\partial \theta}+\frac{\partial^2 V_\theta}{\partial z^2}\right)+q\left(E_0+V_\theta B_0\right)B_0 \tag{3}$$

z-component of Momentum equation:

$$\rho\left(V_r\frac{\partial V_z}{\partial r}+\frac{V_\theta}{r}\frac{\partial V_z}{\partial \theta}+V_z\frac{\partial V_\theta}{\partial z}\right)=-\frac{\partial P}{\partial z}+\rho g_z+\mu\left(\frac{\partial^2 V_z}{\partial r^2}+\frac{1}{r}\frac{\partial V_z}{\partial r}+\frac{1}{r^2}\frac{\partial^2 V_z}{\partial \theta^2}+\frac{\partial^2 V_z}{\partial z^2}\right) \\ +q\left(E_0+V_z B_0\right)B_0 \tag{4}$$

Lorenz Force acting in the counter effect on flow [28] is obtained as follows [29].

$$\overrightarrow{F}=\vec{j}x\overrightarrow{B_0} \tag{5}$$

While the $\vec{j}$ (A/m^2) symbolizes the current density [29] given in Eq. (6) and obtained from Ohm's law. $\overrightarrow{B_0}$ (T) denotes *MF* intensity derived from Maxwell's equations.

$$\vec{j}=\sigma\left(\vec{E}+\vec{V}\times\overrightarrow{B_0}\right) \tag{6}$$

where σ (S/m), $\vec{E}$ (V/m), and $\vec{V}$ (m/s) describe the electrical conductivity of *FF*, electric field, and *HTF* velocity, respectively. The Lorentz force, also known as the magnetic field force, is solved with the Navier-Stokes equations. In this scope, the *MHD* equation [30, 31] defined by Ohm's law and Maxwell's Equations and given in Eq. (7) is solved to be able to calculate the *MHD* effect.

$$\left(\vec{V}\cdot\nabla\right)\vec{B}_0=\frac{1}{\mu\sigma}\nabla^2\vec{B}_0+\left(\overrightarrow{B_0}\cdot\nabla\right)\vec{V} \tag{7}$$

The energy equation used for single-phase numerical solutions is given in Eq. (8) [32]. As in the momentum equation, the heat is generated as a result of applying a *MF* and passing an electric current through conductive materials should also be included in the energy equation. This effect, which is included in the literature as the term Joule Heating [33], is expressed by Eq. (9) and added to the right side of Eq. (11) in scope of *MHD*.

$$\rho c_v\left(V_r\frac{\partial T}{\partial r}+\frac{V_\theta}{r}\frac{\partial T}{\partial \theta}+V_z\frac{\partial T}{\partial z}+\frac{\partial T}{\partial t}\right)=k\left(\frac{\partial^2 T}{\partial r^2}+\frac{1}{r}\frac{\partial T}{\partial r}+\frac{1}{r^2}\frac{\partial^2 T}{\partial \theta^2}+\frac{\partial^2 T}{\partial z^2}\right)+\mu\Phi \tag{8}$$

$$Q=\frac{1}{\sigma}\vec{j}\vec{j} \tag{9}$$

where Φ (W/m^3) is the dissipation energy, which indicates the consumed power against viscous forces.

3.2. Thermophysical properties of Fe_3O_4/H_2O Ferrofluid and data reduction

In this study, Fe_3O_4 *NPs* dispersed with φ=1.0% and 2.0% in H_2O, and pure H_2O were used as *HTF*. The basic thermophysical properties of H_2O and Fe_3O_4 *NP* at T=300 K are given in Table 2. To calculate the thermophysical properties of *FF*, well-known correlations in literature have been used. These thermo-physical properties calculation equations and data reduction equations to be used to evaluate the numerical analysis results are given in Table 3.

Table 2. Thermophysical properties of H_2O and Fe_3O_4 *NP* [16, 34].

Fluid/Particle	**Density, ρ (kg/m^3)**	**Thermal conductivity, k (W/mK)**	**Dynamic viscosity, μ_{HTF}, ($Pa.s$)**	**Specific heat, c_p (J/kgK)**	**Magnetic permeability, μ (H/m)**	**Electrical conductivity, σ, (S/m)**
H_2O	998	0.600	1.003x10^{-3}	4182	1.25e^{-6}	0.05
Fe_3O_4	5180	80.4	-	670	8.80e^{-6}	25000

Table 3. Data reduction equations used in the study.

Parameter	**Equation**	**Reference**	**Equation number**
Density [kg/m^3]	$\rho_{nf} = (1-\varphi)\rho_{bf} + \varphi\rho_{np}$	[35]	(10)
Thermal conductivity [W/mK]	$\frac{k_{nf}}{k_{bf}} = \frac{k_{np} + 2k_{bf} - 2\varphi(k_{bf} - k_{np})}{k_{np} + 2k_{bf} + \varphi(k_{bf} - k_{np})}$	[36]	(11)
Dynamic viscosity [Pa.s]	$\frac{\mu_{nf}}{\mu_{bf}} = (1 + 7.3\varphi + 123\varphi^2)$	[37]	(12)
Specific heat [J/kgK]	$c_{p_{nf}} = \frac{(1-\varphi)(\rho c_p)_{bf} + \varphi(\rho c_p)_{np}}{\rho_{nf}}$	[38]	(13)
Reynolds number [-]	$\mathrm{Re} = \frac{\rho V D}{\mu_{HTF}}$	[39]	(14)
Heat convection coefficient [W/m^2K]	$h = \frac{q''}{(T_w - T_b)}$	[39]	(15)
Bulk temperature [K]	$T_b = \frac{T_{in} + T_{out}}{2}$	[39]	(16)
Nusselt number [-]	$Nu = \frac{hD}{k}$	[40]	(17)
Darcy friction factor [-]	$ff = \frac{\Delta P}{\left(\frac{L}{D}\right)\left(\frac{\rho V^2}{2}\right)}$	[41]	(18)
Performance Evaluation Criterion [-]	$PEC = \frac{\left(\frac{Nu_{enhanced}}{Nu_{base}}\right)}{\left(\frac{ff_{enhanced}}{ff_{base}}\right)^{1/3}}$	[42]	(19)

3.3. Solution method

The iterative solutions have been conducted via ANSYS Fluent 2020 R2 software. Single-phase fluid properties have been accepted for the analyses. Whereas the no-slip condition has been assumed for all tube walls, the heat flux of q''=600 W/m^2 has been just applied to the outlet tube. Analyses have been conducted using the steady-state flow condition. Pressure-based solver has been used for the solutions. Also, absolute velocity formulation has been assumed. The SIMPLE algorithm has been preferred as a pressure-velocity coupling method due to being faster than other solvers. As the Spatial Discretization, Squares Cell Based, Second Order, and Second Order Upwind methods have been used as the discrimination of the governing equations.

4. Mesh Independency Study and Validation

Since the element number of a mesh directly affects the solution time, the mesh independency study must be performed for the fluid domain to obtain the optimum element number [43]. For this purpose, the analysis has been carried out under *Re*=1000 using H_2O as the *HTF*. The fluid domain has meshed using global and local mesh settings to reach the suitable mesh quality. After that, mesh independency analyses have been conducted using variable mesh values. The *Nu* and *ff* results obtained from various mesh element numbers are presented in Fig. 3. It is seen that the results exhibited stability after the 2499684 element numbers. The mesh settings at this point have been approved as the base mesh settings for all fluid domains. The obtained mesh structures are presented in Fig. 4.

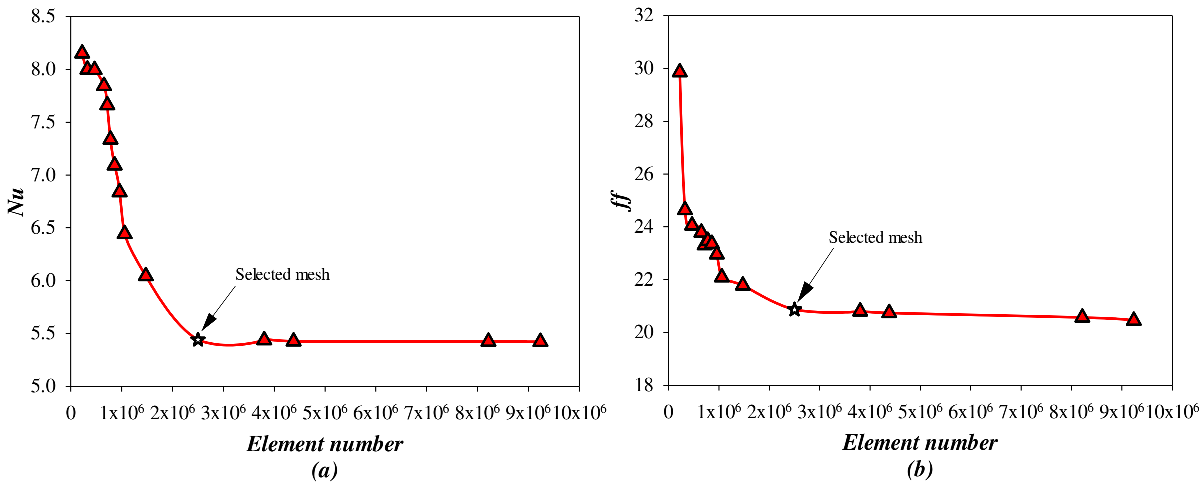

Fig. 3. Mesh independency results for *Re*=1000 using H_2O; (a) *Nu*, (b) *ff*.

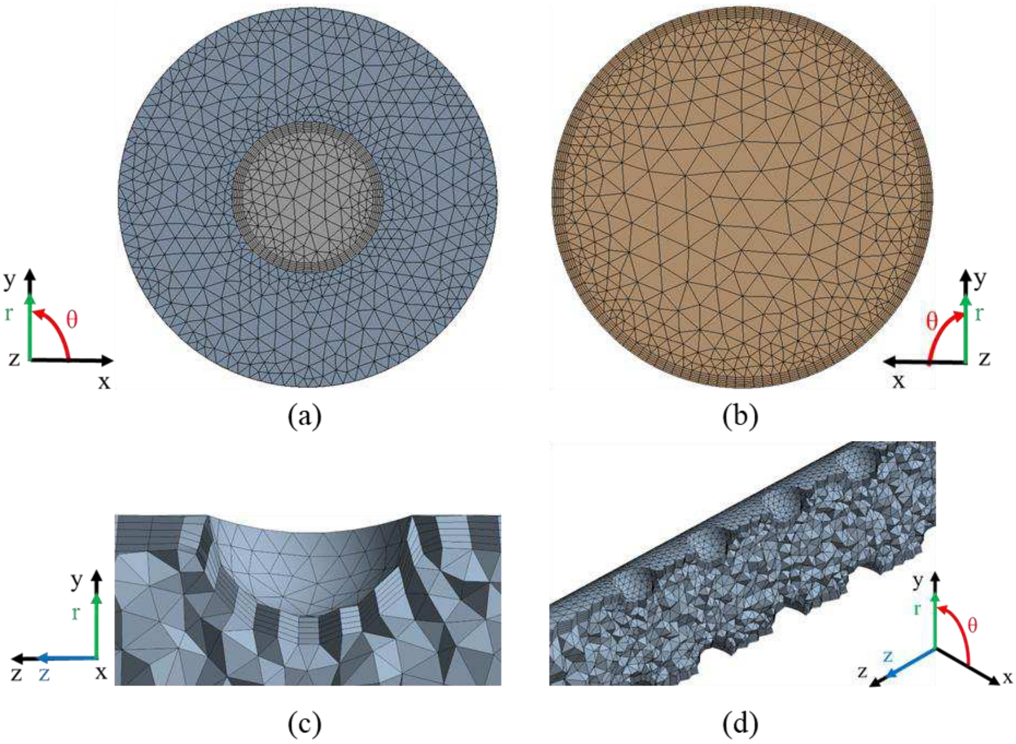

Fig. 4. Base mesh structures at; (a) inlet section, (b) outlet section, (c) *DF* side, and (d) longitudinal view.

To demonstrate the validity of the analyses, the results have been compared with previously published studies in the literature. For this purpose, the fluid domain without *DF* has been formed and results have been obtained at *Re*=290 using H_2O as *HTF*. As a result of this, the numerical results have been compared with Ref. [44]. The validation has been carried out with the help of the velocity profile given in Fig. 5 at the sudden expansion point (*z*=375 *mm*). It is concluded that there is a good agreement between the present study and the data obtained from the literature.

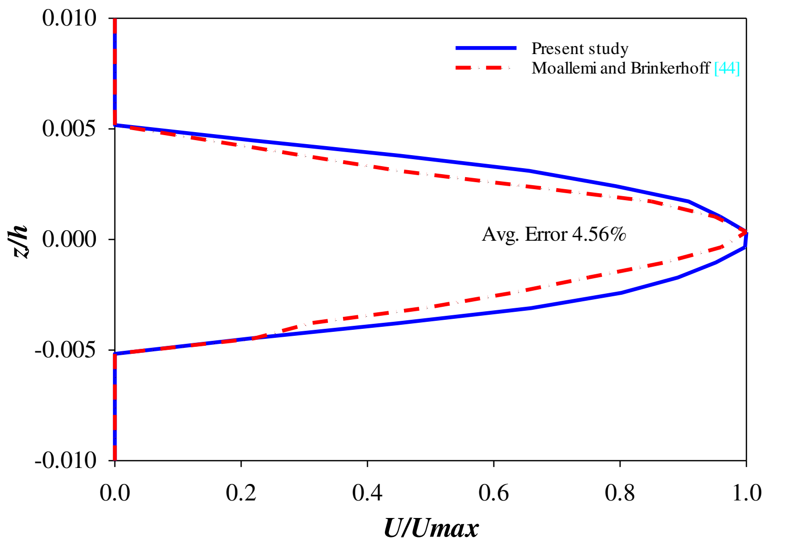

Fig. 5. Validation of the results with literature using velocity profile at *z*=375 *mm*.

5. Results and Discussion

5.1. Effect of dimple fin and ferrofluid on heat transfer and flow characteristics

The effect of *DF* and Fe_3O_4/H_2O *FF* on *THP* has comprehensively been given in Fig. 6. Generally, the average *Nu* and average *ff* exhibit an increment and decrement as the increment of *Re*, respectively. Moreover, the average *Nu* and *ff* show a rising up in the case of using *DT* compared to *ST*. For example, the average *Nu* presents an enhancement of 22.62% whereas an increase of 3.28% is realized for the average *ff* at *Re*=2000. When investigating the effect of Fe_3O_4/H_2O *FF* on *THP*, the average *Nu* shows an augmentation of 5.43% and 6.27% for φ=1.0% and 2.0%, respectively compared to H_2O at *Re*=2000. Furthermore, a drastic soaring is realized in *ff* as 3.16% and 3.21% for φ=1.0% and 2.0% at *Re*=2000, respectively. It is concluded that using *DT* is more effective than using Fe_3O_4/H_2O *FF* in terms of heat transfer enhancement, and this result is supported in a study published by Pourfattah et al. [45]. In the case of using *DT* and 2.0% Fe_3O_4/H_2O *FF*, 30.31% raise is observed for average *Nu* at *Re*=2000 while an boost of 6.60% is occurred for average *ff*.

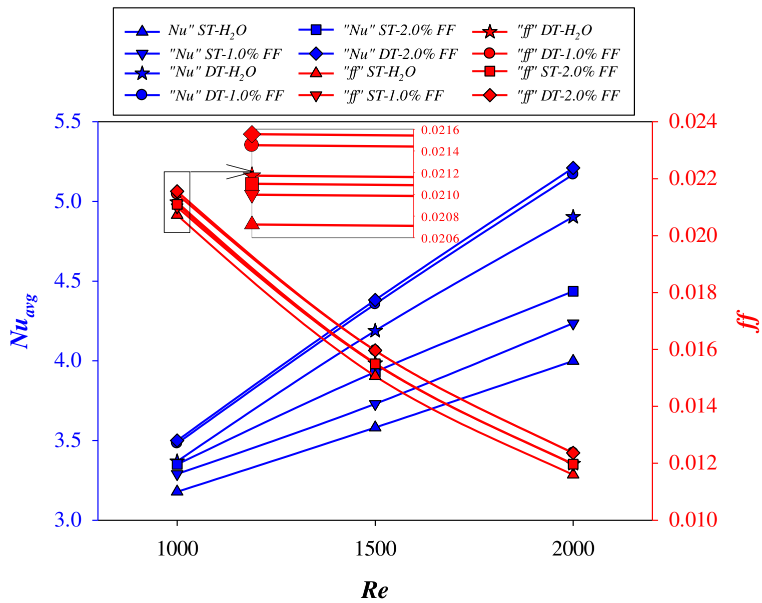

Fig. 6. Variation of average *Nu* and *ff* with *Re* under *DT* and *FF* effect.

It has already been mentioned that the presence of *DF* is more efficient than the use of *NF* for enhancing heat transfer. To demonstrate the heat transfer and flow characteristics mechanism of *DT*, a visual description is presented in Fig. 7 (a-c). In Fig. 7 (a), the streamlines and local *Nu* distribution are shown flowing through the tube. While the *HTF* flows in the *DF* at *Re*= 2000, *HTF* impinges the upstream side of the *DF*, and flow is interrupted. The velocity profile is approached to the center of the tube due to the effect of this interruption, and flow separation is formed on the upstream side of *DF* [46]. This phenomenon positively affects the flow in terms of *THP* by thinning the velocity boundary layer. As a result, the pressure and inertia forces are more dominant than the viscous force, and the thermal boundary layer thickness becomes thinner [47]. Thus, the *THP* of the *SET* exhibits an enhancement as the decrement of the field synergy angle (α) [48]. As the *HTF* flows over the protrusion section of the *DF*, an increase in *HTF's* velocity takes place due to narrower cross-section, and then the *HTF* spreads over a larger volume. Due to this spread, secondary flow occurs, which prevents the convection of heat flux applied downstream of the *DF* to the *HTF*. Furthermore, Fig. 7 (b) and (c) show the comparison of local *Nu* distribution on outlet tubes for *ST* and *DT*. As can be seen from the figures, *DT* provides superiority over *ST* in terms of convective heat transfer thanks to the enhancement in local *Nu* values. Fig. 7 (c) explicitly presents the difference of top and bottom walls in terms of surface *Nu* distribution. According to the contours, the top wall realizes more heat transfer than the bottom wall for judging by the entire tube and this result presents similarity with the data in Ref. [49].

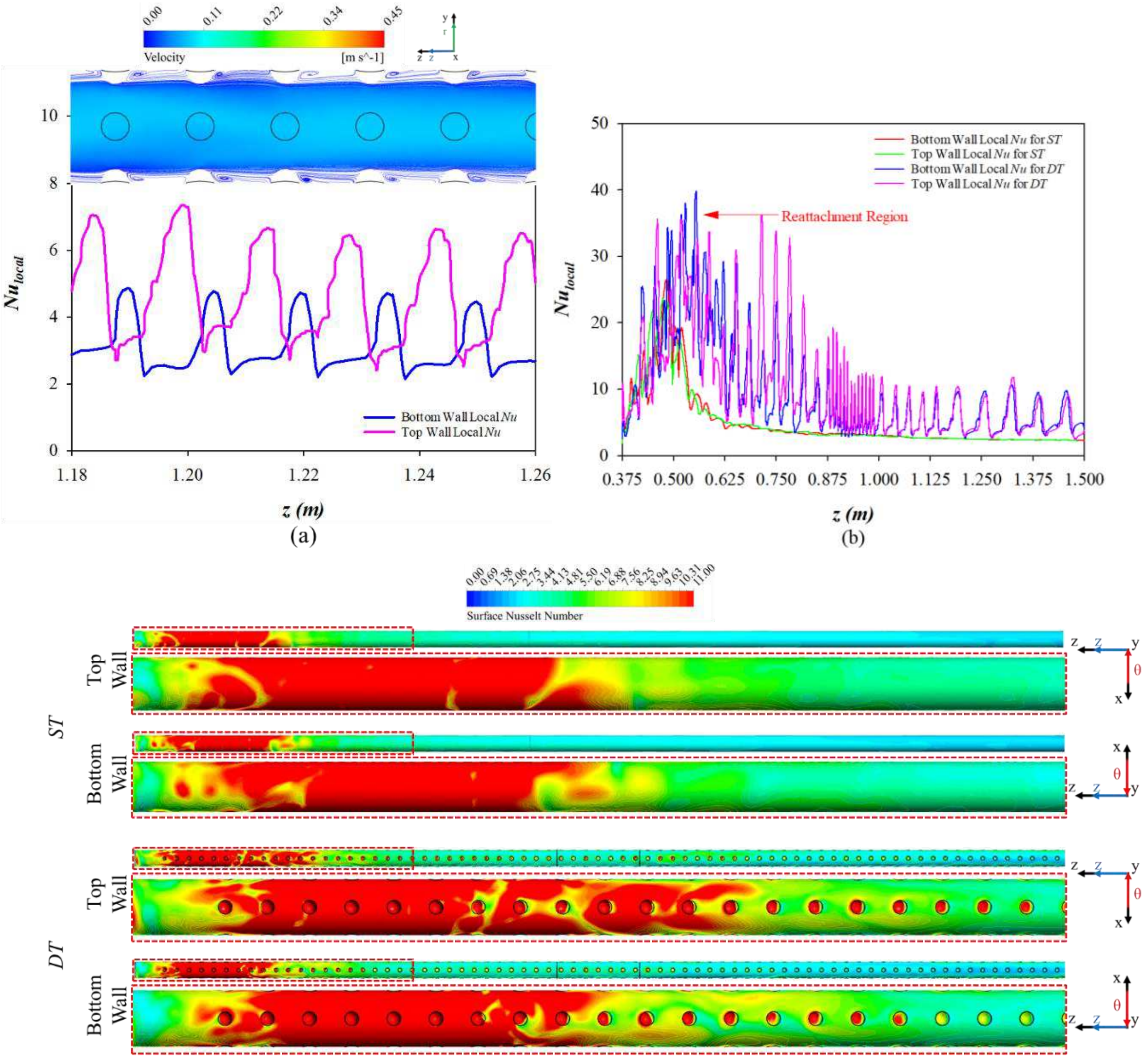

Fig. 7. Effect of *DF* on *THP* at *Re*=2000; (a) interaction of heat transfer and flow characteristics in *DT*, (b) comparison to Nu_{local} in *ST* and *DT* as a trend (c) comparison to Nu_{local} distribution in *ST* and *DT*.

Investigation of the *PEC* presents the applicability and feasibility of the designed thermal system. Within the scope of this concept, the *PEC* results have been presented in Fig. 8 to exhibit the *THP*. The trends show that obtained thermal performance using the *DF* and *FF* come to the forefront compared to the adverse effect of hydraulics. Besides, it is seen that the using *DF* dominates the using Fe_3O_4/H_2O *FF* in terms of *THP*. When the evaluation has made for *DF* alone, it was determined that *PEC* rises by 21.31% at *Re*=2000. When the evaluation has made for Fe_3O_4/H_2O *FF* alone, it was determined that *PEC* soars by 4.85% and 9.79% at *Re*=2000 for φ=1.0% and 2.0%, respectively. In the case of the use of *DF* and *FF* together, *PEC* exhibits an increment of 26.58% and 27.56% at *Re*=2000 for φ=1.0% and 2.0%, respectively.

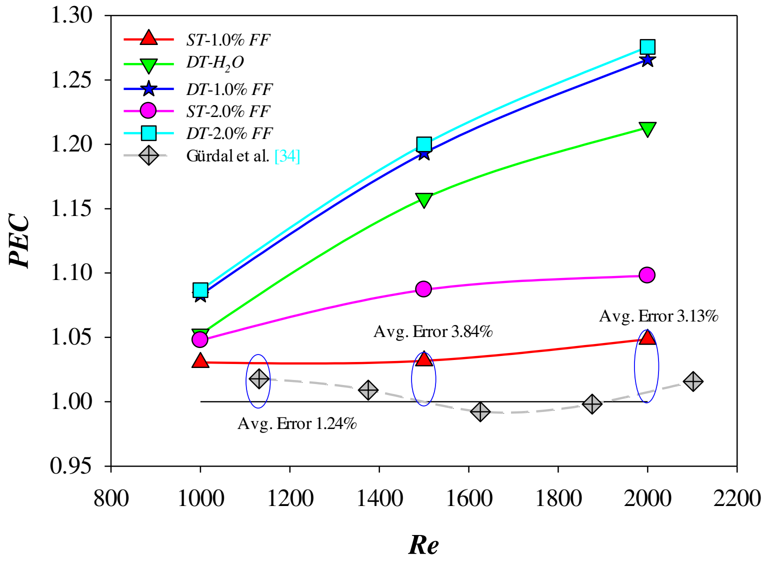

Fig. 8. Variation of *PEC* with *Re* under *DT* and *FF* effect.

The increment in convective heat transfer that occurs with the use of Fe_3O_4/H_2O *FF* has been attributed to the Brownian motion and Thermophoresis phenomena, which are also referred to as slip mechanisms by many researchers [50, 51]. The Brownian motion defines as the random motion of *NPs* and collides of these *NPs* with each other. As a result of this interaction, heat is transferred from one *NP* to another. While the *NP* flows in the *HTF*, heat transfer realizes in two different ways. The first phenomenon is called direct contribution, which can explain by the heat transfer among the *NPs*. In contrast, the second phenomenon is called indirect contribution (micro-convection), which is realized between *NP* and *HTF* that surrounds the *NP* [52]. The Brownian motion disrupts the thermal boundary layer, and this phenomenon contributes to enhancing the convective heat transfer performance of the system [53]. Another effect is the Thermophoresis phenomenon (also known as the Soret effect [54]), which has been studied by many researchers and is claimed to be worth investigating [55, 56]. Thermophoresis can be defined as the time-averaged force formed by the Brownian motion of the *NPs* in the *HTF* under the influence of temperature gradient [57]. With the effect of this force, the particles in the hot region of the flow area tend to flow toward the cold regions. Because the Thermophoretic force, which is proportional to the temperature gradient, has higher values in the higher temperature gradient [58].

5.2. Effect of magnetic field on heat transfer and flow characteristic

The application of the *MF* in a *SET* put forward the novelty of this study. Within this scope, different *DC MF* intensities (B_0=0.03*T*, 0.05*T*, 0.3*T*, and 0.5*T*) have been applied on the outlet tube wall at *z*=937.5 *mm*. The *THP* behavior of *DT* in both presence and absence of *MF* is given in Fig. 9. The results exhibit a closeness to each other. However, it can be mentioned that as the intensity of *MF* growths, the average *Nu* and average *ff* show an increase. The highest average *Nu* has been obtained as 5.28 for the case of B_0=0.5*T* and *Re*=2000 using φ=2.0% Fe_3O_4 *FF*. When a comparison is carried out between *DC MF* intensities and the absence of *MF*, the average *Nu* performs an increment of 0.42%, 0.74%, 1.22%, and 1.42% for B_0=0.03*T*, 0.05*T*, 0.3*T*, and 0.5*T*, respectively. On the other hand, the average *ff* tends to decrease with the increment of *Re*, gradually. Compared to the absence of *MF*, the average *ff* shows an increment of 0.30%, 0.50%, 1.30%, and 2.50% for B_0=0.03*T*, 0.05*T*, 0.3*T*, and 0.5*T*, respectively.

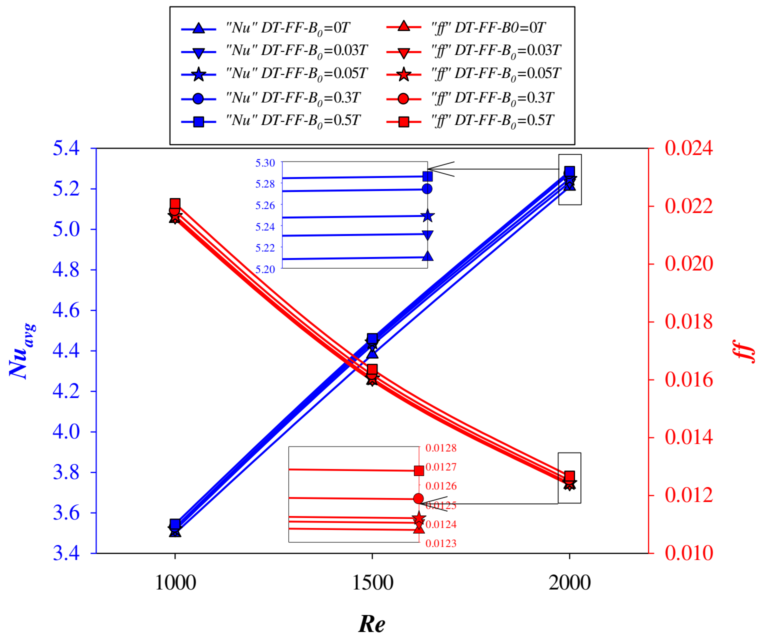

Fig. 9. Variation of average *Nu* and *ff* with *Re* under different *DC MF* intensities.

Many factors can explain the variation in the *THP* of the system with the application of *MF*. The one of the most important effects is the Lorentz force, which occurs due to the electrical conductivity of the *HTF*. Based on the *MHD*, when an external *MF* is applied to the magnetizable *NPs*, creates an effect called the Lorentz force between the fluid and the *MF* source [59]. The Lorentz force acts *HTF* flow at the opposite direction, which causes occurrence of vortex in the *MF* applied region [34, 60]. Another factor affecting *THP* is the magnetophoresis transport mechanism [61] formed by Fe_3O_4 *NP* acting in *MF*. Magnetophoresis is a heterogeneous behavior from quasi-homogeneous behavior when magnetizable *NPs* such as Fe_3O_4 *NP* are attracted to the tube´s wall under the influence of an *MF*. The *NPs* are attracted to the tube's wall and disperse the boundary layers there leading an increase in heat transfer rate.

The effect of *DC MF* on *PEC* is presented in Fig. 10 using Fe_3O_4/H_2O *FF* with φ=2.0%. According to the results, the *PEC* shows an increment up to B_0=0.3*T*. When the Fe_3O_4/H_2O *FF* is subjected to B_0=0.5*T DC MF*, the *PEC* exhibits a decrement. A similar result has been acquired by Ghofrani et al. [62] and Yarahmadi et al. [63]. When a detailed investigation carries out on the results, it is obtained that the *PEC* of Fe_3O_4/H_2O *FF* flowing in *DT* performs an increment of 27.97%, 28.30%, 28.57%, and 28.31% with exposed to B_0=0.03*T*, 0.05*T*, 0.3*T*, and 0.5*T DC MF*, respectively.

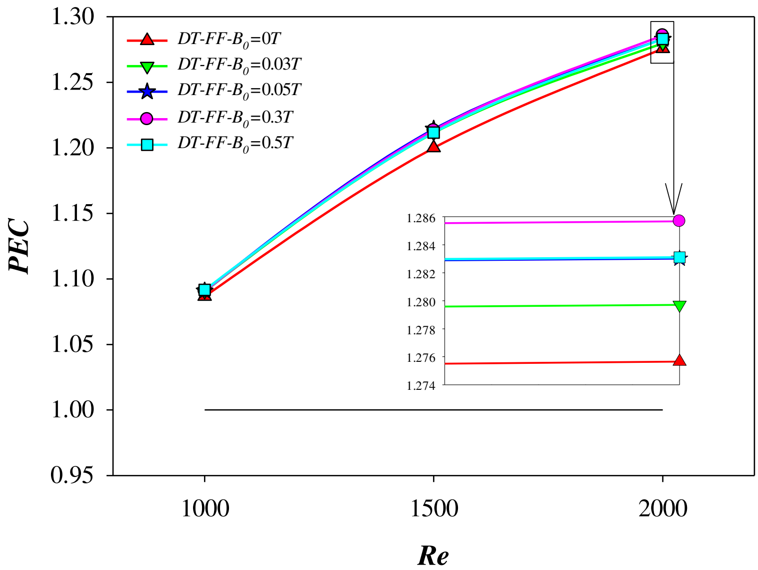

Fig. 10. Variation of *PEC* with *Re* under different *DC MFs* intensities.

To demonstrate the *DC MF* effect on heat transfer, the surface *Nu* distribution at *MF* applied surface is presented in Fig. 12 for B_0=0*T* and 0.3*T DC MFs* at φ=2.0% and *Re*=2000. The surface *Nu* distributions are demonstrated for *x* and -*x* direction surfaces. The distributions show that *MF* has a positive effect on heat transfer not only on the *MF* applied surface but also after this region. The main reason underlying this result is based on the effect of *MF* on flow motion.

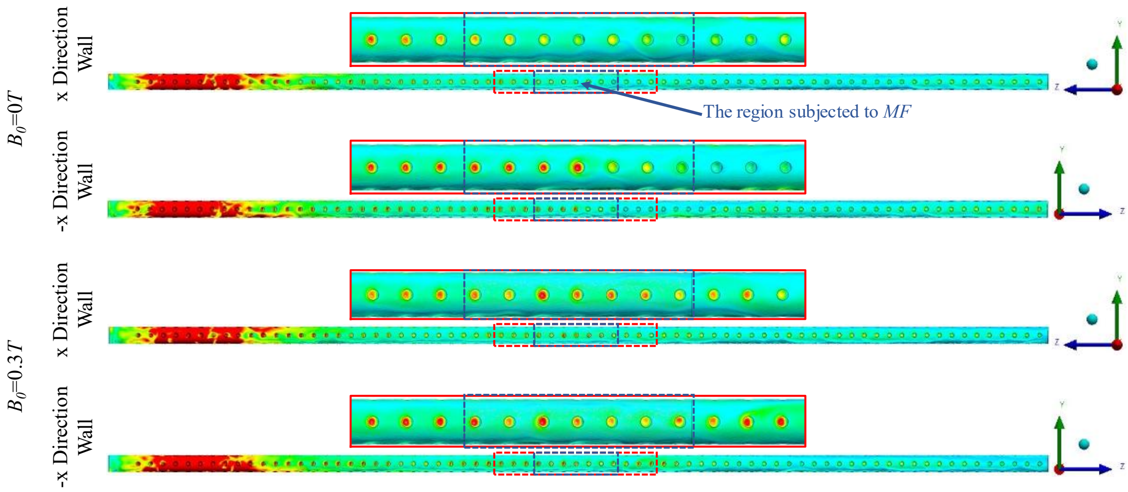

Fig. 12. Exhibiting the surface *Nu* distribution.

The effect of *DC MF* on temperature gradient and vorticity formation at *Re*=2000 and *z*=927.5 *mm* is presented in Fig. 13. It can be seen that along with increments of the *DC MF* intensity, the temperature gradient becomes a more uniform situation shown in Fig 13 (a). However, the same explanation cannot be made for the vorticity formation given in Fig. 13 (b). As the *DC MF* intensity increases, no visible change in vorticity formation is observed.

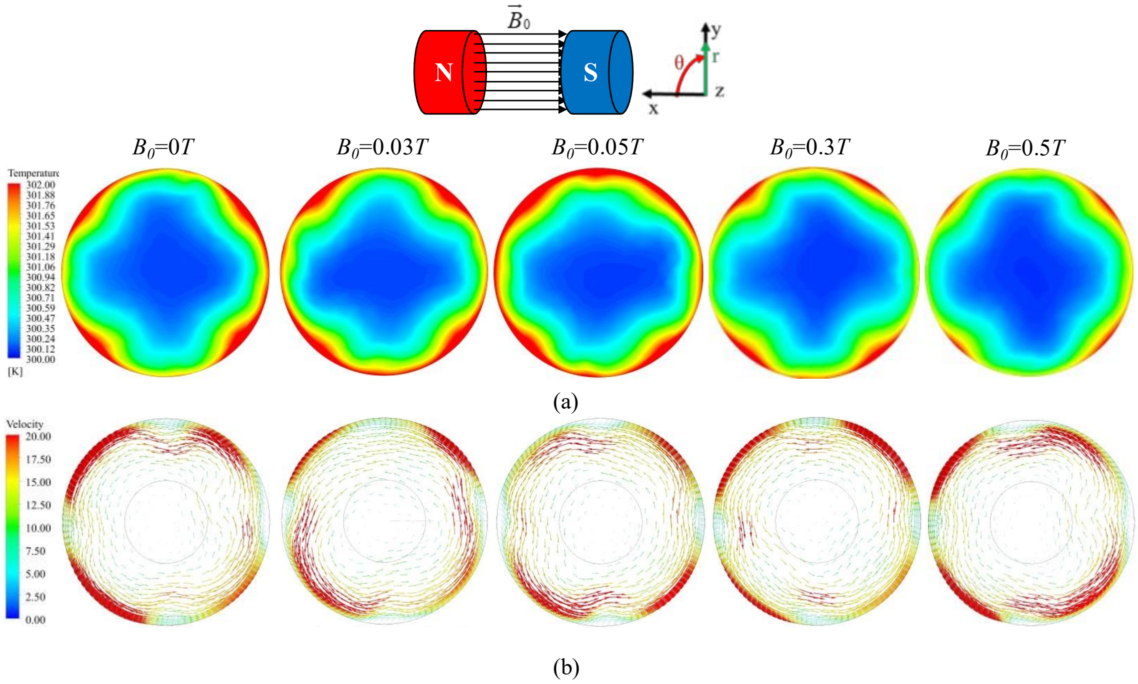

Fig. 13. *DC MF* effect on (a) temperature gradient and (b) vorticity formation.

6. Conclusions

In this study, the influence of the compound heat transfer enhancement techniques, which include *DF*, *NF*, and *MF* is detailly investigated in *SET* to determine the *THP* effect. The result of average *Nu*, local *Nu*, average *ff*, local *ff*, average velocity, local velocity, and *PEC* are presented with graphs while surface *Nu* distribution on *DT* and *DC MF* applied regions, temperature gradient, and vorticity formation at *DC MF* region are tackled, in detail. The following remarks can be summarized below.

- The average *Nu* and *ff* show an increment of 22.62% and 3.28% in *DT* compared to *ST* using H_2O at *Re*=2000.
- Using Fe_3O_4/H_2O *FF* shows an enhancement of 5.43% and 6.27% in average *Nu* for φ=1.0% and 2.0%, respectively, compared to H_2O in the same conditions. Besides, Fe_3O_4/H_2O *FF* increments the average *ff* by 3.16% and 6.27% compared to H_2O, respectively.
- The use of *DF* provides a 21.31% increment in *PEC*, while the use of Fe_3O_4/H_2O *FF* with φ=1.0% and 2.0% results in an increment of 4.85% and 9.79%, respectively.
- The results represent that using *DF* is more effective than Fe_3O_4/H_2O *FF* in terms of *THP*.
- The highest average *Nu* is obtained in B_0=*0.5T DC MF*. However, the highest *PEC* is acquired in B_0=*0.3T DC MF*.
- When investigating the *PEC* results in applied *DC MF*, increments of 27.97%, 28.30%, 28.57%, and 28.31% are realized in Fe_3O_4/H_2O *FF* flowing through *DT* exposed to B_0=0.03*T*, 0.05*T*, 0.3*T*, and 0.5*T DC MF*, respectively.
- Noteworthy and explicit visual results have been obtained in *DF* and *MF* effects.

CRediT author statement

Emrehan Gürsoy: Conceptualization, Methodology, Validation, Formal analysis, Investigation, Data Curation, Writing-Original Draft, Writing - Review & Editing, Visualization.

Hayati Kadir Pazarlıoğlu: Conceptualization, Methodology, Validation, Data Curation, Writing - Review & Editing, Supervision, Visualization.

Mehmet Gürdal: Conceptualization, Methodology, Validation, Data Curation, Writing-Original Draft, Writing - Review & Editing, Supervision, Visualization.

Kamil Arslan: Methodology, Writing - Review & Editing, Supervision, Project Administration.

Engin Gedik: Conceptualization, Methodology, Writing - Review & Editing, Supervision, Project Administration.

Addullah Dağdeviren: Visualization.

Funding

Emrehan Gürsoy has been supported by TÜBİTAK BİDEB-2211/C fellowship in the scope of this study.

References

1. Mountford H, Waskow D, Gonzalez L, et al (2021) COP26: key outcomes from the un climate talks in glasgow
2. Lennan M, Morgera E (2022) The Glasgow Climate Conference (COP26). Int J Mar Coast Law

37:137–151

3. Mahian O, Bellos E, Markides CN, et al (2021) Recent advances in using nanofluids in renewable energy systems and the environmental implications of their uptake. Nano Energy 86:106069. https://doi.org/10.1016/J.NANOEN.2021.106069
4. Sharma P, Said Z, Kumar A, et al (2022) Recent advances in machine learning research for nanofluid-based heat transfer in renewable energy system. Energy & Fuels 36:6626–6658
5. Dizaji HS, Pourhedayat S, Aldawi F, et al (2022) Proposing an innovative and explicit economic criterion for all passive heat transfer enhancement techniques of heat exchangers. Energy 239:122271. https://doi.org/10.1016/J.ENERGY.2021.122271
6. Thapa S, Samir S, Kumar K, Singh S (2021) A review study on the active methods of heat transfer enhancement in heat exchangers using electroactive and magnetic materials. Mater Today Proc 45:4942–4947. https://doi.org/10.1016/J.MATPR.2021.01.382
7. Suri ARS, Pun AK, Al Haque MS (2022) Review of heat transfer augmentation methods and effect of using dimpled ribs and nanofluids. Mater Today Proc 50:830–836. https://doi.org/10.1016/J.MATPR.2021.05.702
8. Gürdal M, Arslan K, Gedik E, Minea AA (2022) Effects of using nanofluid, applying a magnetic field, and placing turbulators in channels on the convective heat transfer: A comprehensive review. Renew Sustain Energy Rev 162:112453. https://doi.org/10.1016/J.RSER.2022.112453
9. Malapur H V., Havaldar SN, Anderson GA (2023) Heat gain in an internally dimpled tube heat exchanger - a numerical investigation. Mater Today Proc 72:1530–1536. https://doi.org/10.1016/J.MATPR.2022.09.382
10. Dagdevir T (2022) Multi-objective optimization of geometrical parameters of dimples on a dimpled heat exchanger tube by Taguchi based Grey relation analysis and response surface method. Int J Therm Sci 173:107365. https://doi.org/10.1016/J.IJTHERMALSCI.2021.107365
11. Kaood A, Aboulmagd A, Othman H, ElDegwy A (2022) Numerical investigation of the thermal-hydraulic characteristics of turbulent flow in conical tubes with dimples. Case Stud Therm Eng 36:102166. https://doi.org/10.1016/J.CSITE.2022.102166
12. Zheng J, Liang Z, Zhang L, et al (2023) Forming experiment of extruded tube with crossed ellipsoidal dimples and numerical investigation on heat transfer enhancement and flow characteristics. Int Commun Heat Mass Transf 141:106599. https://doi.org/10.1016/J.ICHEATMASSTRANSFER.2022.106599
13. Abderrahmane A, Hatami M, Medebber MA, et al (2022) Non-Newtonian nanofluid natural convective heat transfer in an inclined Half-annulus porous enclosure using FEM. Alexandria Eng J 61:5441–5453. https://doi.org/10.1016/J.AEJ.2021.11.004
14. Strandberg R, Das DK (2010) Finned tube performance evaluation with nanofluids and conventional heat transfer fluids. Int J Therm Sci 49:580–588. https://doi.org/10.1016/J.IJTHERMALSCI.2009.08.008

15. Lenert A, Nam Y, Wang EN (2012) HEAT TRANSFER FLUIDS. Annu Rev Heat Transf 15:45. https://doi.org/10.1615/ANNUALREVHEATTRANSFER.2012004122
16. Gürsoy E, Kadir Pazarlıoğlu H, Dağdeviren A, et al (2022) Energy analysis of magnetite nanofluid flowing in newly designed sudden expansion tube retrofitted with dimpled fin. Int J Heat Mass Transf 199:123446. https://doi.org/10.1016/J.IJHEATMASSTRANSFER.2022.123446
17. Ahmad F, Mahmud S, Ehsan MM, Salehin M (2023) Thermo-hydrodynamic performance evaluation of double-dimpled corrugated tube using single and hybrid nanofluids. Int J Thermofluids 17:100283. https://doi.org/10.1016/J.IJFT.2023.100283
18. Apmann K, Fulmer R, Soto A, Vafaei S (2021) Thermal conductivity and viscosity: Review and optimization of effects of nanoparticles. Materials (Basel) 14:1291
19. Mousa MH, Miljkovic N, Nawaz K (2021) Review of heat transfer enhancement techniques for single phase flows. Renew Sustain Energy Rev 137:110566. https://doi.org/10.1016/J.RSER.2020.110566
20. Gürdal M, Pazarlıoğlu HK, Tekir M, et al (2022) Implementation of hybrid nanofluid flowing in dimpled tube subjected to magnetic field. Int Commun Heat Mass Transf 134:106032. https://doi.org/10.1016/J.ICHEATMASSTRANSFER.2022.106032
21. Shahsavar A, Askari IB, Ghodrat M, et al (2023) Experimental investigation of the effect of mechanical vibration and rotating magnetic field on the hydrothermal performance of water-Fe3O4 ferrofluid inside a rifled tube. J Magn Magn Mater 170586. https://doi.org/https:/doi.org/10.1016/j.jmmm.2023.170586
22. Halawa T, Tanious AS (2023) Investigation of the optimum design of magnetic field arrangement to enhance heat transfer performance of Fe3O4-water magnetic nanofluid. Int J Therm Sci 184:108014. https://doi.org/10.1016/J.IJTHERMALSCI.2022.108014
23. Tekir M, Taskesen E, Aksu B, et al (2020) Comparison of bi-directional multi-wave alternating magnetic field effect on ferromagnetic nanofluid flow in a circular pipe under laminar flow conditions. Appl Therm Eng 179:115624. https://doi.org/10.1016/j.applthermaleng.2020.115624
24. Çengel YA, Cimbala JM (2018) Fluid Mechanics A Fundamental Approach
25. Hosseinzadeh K, Erfani Moghaddam MA, Nateghi SK, et al (2023) Radiation and convection heat transfer optimization with MHD analysis of a hybrid nanofluid within a wavy porous enclosure. J Magn Magn Mater 566:170328. https://doi.org/10.1016/J.JMMM.2022.170328
26. Jiji LM (2009) Heat Convection, Second Edi. Springer, New York
27. Lim JH, Park M (2022) Studies on Heat Transfer Coefficient of a Circular Tube With Twisted Tape Insert for High Heat Flux Cooling Applications; Studies on Heat Transfer Coefficient of a Circular Tube With Twisted Tape Insert for High Heat Flux Cooling Applications. IEEE Trans Plasma Sci 50:459. https://doi.org/10.1109/TPS.2022.3141820

28. Jalili B, Sadighi S, Jalili P, Ganji DD (2022) Numerical analysis of MHD nanofluid flow and heat transfer in a circular porous medium containing a Cassini oval under the influence of the Lorentz and buoyancy forces. Heat Transf 51:6122–6138
29. Manna NK, Biswas N, Mandal DK, et al (2023) Impacts of heater-cooler position and Lorentz force on heat transfer and entropy generation of hybrid nanofluid convection in quarter-circular cavity. Int J Numer Methods Heat Fluid Flow 33:1249–1286
30. Antonov AA (2015) Adjustment of the special theory of relativity according to the Ohm's law. Am J Electrical Electron Engineeing 3:124–129
31. Maxwell JC (1873) A treatise on electricity and magnetism. Oxford: Clarendon Press
32. Bejan A (2013) Convection heat transfer, Fourth Edi. John Wiley & Sons, Inc., Durham, North Carolina
33. Zhang J-K, Li B-W, Chen Y-Y (2015) The joule heating effects on natural convection of participating magnetohydrodynamics under different levels of thermal radiation in a cavity. J Heat Transfer 137:
34. Gürdal M, Pazarlıoğlu HK, Tekir M, et al (2022) Numerical investigation on turbulent flow and heat transfer characteristics of ferro-nanofluid flowing in dimpled tube under magnetic field effect. Appl Therm Eng 200:117655. https://doi.org/10.1016/J.APPLTHERMALENG.2021.117655
35. Shafiq M, Farooq M, Javed W, et al (2023) Thermo-Hydraulic Performance Analysis of Fe3O4-Water Nanofluid-Based Flat-Plate Solar Collectors. Sustainability 15:4704
36. Afshari F, Muratçobanoğlu B (2023) Thermal analysis of Fe3O4/water nanofluid in spiral and serpentine mini channels by using experimental and theoretical models. Int J Environ Sci Technol 20:2037–2052. https://doi.org/10.1007/s13762-022-04119-6
37. Eshgarf H, Ahmadi Nadooshan A, Raisi A, Afrand M (2023) Experimental examination of the properties of Fe3O4/water nanofluid, and an estimation of a correlation using an artificial neural network. J Mol Liq 374:121150. https://doi.org/10.1016/J.MOLLIQ.2022.121150
38. Afshari F, Mandev E, Rahimpour S, et al (2023) Experimental and numerical study on air-to-nanofluid thermoelectric cooling system using novel surface-modified Fe3O4 nanoparticles. Microfluid Nanofluidics 27:26
39. Çengel YA, Ghajar AJ (2015) Heat and Mass Transfer Fundamentals & Applications
40. Kia S, Khanmohammadi S, Jahangiri A (2023) Experimental and numerical investigation on heat transfer and pressure drop of SiO2 and Al2O3 oil-based nanofluid characteristics through the different helical tubes under constant heat fluxes. Int J Therm Sci 185:108082. https://doi.org/10.1016/J.IJTHERMALSCI.2022.108082
41. Gürdal M (2023) Artificial intelligence approach for energy and entropy analyses of NiFe2O4/H2O nanofluid flow in a tube with vortex generator. Eng Anal Bound Elem 152:277–292. https://doi.org/10.1016/J.ENGANABOUND.2023.04.016

42. Taskesen E, Tekir M, Gedik E, Arslan K (2021) Numerical investigation of laminar forced convection and entropy generation of Fe3O4/water nanofluids in different cross-sectioned channel geometries. J Therm Eng 7:1752–1767. https://doi.org/10.18186/thermal.1025984
43. Jalili B, Aghaee N, Jalili P, Domiri Ganji D (2022) Novel usage of the curved rectangular fin on the heat transfer of a double-pipe heat exchanger with a nanofluid. Case Stud Therm Eng 35:102086. https://doi.org/10.1016/J.CSITE.2022.102086
44. Moallemi N, Brinkerhoff JR (2016) Numerical analysis of laminar and transitional flow in a planar sudden expansion. Comput Fluids 140:209–221
45. Pourfattah F, Akbari OA, Jafrian V, et al (2020) Numerical simulation of turbulent flow and forced heat transfer of water/CuO nanofluid inside a horizontal dimpled fin. J Therm Anal Calorim 139:3711–3724. https://doi.org/https://doi.org/10.1007/s10973-019-08752-1
46. Zhang L, Xiong W, Liang Z (2021) Effect of outline curvature degree on heat transfer and flow characteristics inside dimpled tubes and spirally grooved tubes. Heat Transf 50:3996–4018
47. Rashidi S, Hormozi F, Sundén B, Mahian O (2019) Energy saving in thermal energy systems using dimpled surface technology – A review on mechanisms and applications. Appl Energy 250:1491–1547. https://doi.org/10.1016/j.apenergy.2019.04.168
48. Li F, Ma Q, Xin G, et al (2020) Heat transfer and flow characteristics of microchannels with solid and porous ribs. Appl Therm Eng 178:115639. https://doi.org/10.1016/J.APPLTHERMALENG.2020.115639
49. Pazarlıoğlu HK, Gürsoy E, Gürdal M, et al (2023) The first and second law analyses of thermodynamics for CoFe2O4/H2O flow in a sudden expansion tube inserted elliptical dimpled fins. Int J Mech Sci 246:108144. https://doi.org/10.1016/J.IJMECSCI.2023.108144
50. Dawar A, Saeed A, Kumam P (2022) Magneto-hydrothermal analysis of copper and copper oxide nanoparticles between two parallel plates with Brownian motion and thermophoresis effects. Int Commun Heat Mass Transf 133:105982. https://doi.org/10.1016/J.ICHEATMASSTRANSFER.2022.105982
51. Kalpana G, Madhura KR, Kudenatti RB (2022) Magnetohydrodynamic boundary layer flow of hybrid nanofluid with the thermophoresis and Brownian motion in an irregular channel: A numerical approach. Eng Sci Technol an Int J 32:101075. https://doi.org/10.1016/J.JESTCH.2021.11.001
52. Nkurikiyimfura I, Wang Y, Pan Z (2013) Heat transfer enhancement by magnetic nanofluids—A review. Renew Sustain Energy Rev 21:548–561. https://doi.org/10.1016/J.RSER.2012.12.039
53. Apmann K, Fulmer R, Scherer B, et al (2022) Nanofluid heat transfer: Enhancement of the heat transfer coefficient inside microchannels. Nanomaterials 12:615
54. Njingang Ketchate CG, Tiam Kapen P, Madiebie-Lambou I, et al (2023) Chemical reaction, Dufour and Soret effects on the stability of magnetohydrodynamic blood flow conveying magnetic nanoparticle in presence of thermal radiation: A biomedical application. Heliyon

9:e12962. https://doi.org/10.1016/J.HELIYON.2023.E12962

55. di Schio E, Celli M, Barletta A (2014) Effects of Brownian diffusion and thermophoresis on the laminar forced convection of a nanofluid in a channel. J Heat Transfer 136:

56. Wang R, Chen T, Qi J, et al (2021) Investigation on the heat transfer enhancement by nanofluid under electric field considering electrophorestic and thermophoretic effect. Case Stud Therm Eng 28:101498. https://doi.org/10.1016/J.CSITE.2021.101498

57. Michaelides EE (2015) Brownian movement and thermophoresis of nanoparticles in liquids. Int J Heat Mass Transf 81:179–187. https://doi.org/10.1016/J.IJHEATMASSTRANSFER.2014.10.019

58. Yin Z-Q, Li X-F, Bao F-B, et al (2018) Thermophoresis and Brownian motion effects on nanoparticle deposition inside a 90 square bend tube. Aerosol Air Qual Res 18:1746–1755. https://doi.org/10.4209/aaqr.2018.02.0047

59. Sheikholeslami M, Saleem S, Shafee A, et al (2019) Mesoscopic investigation for alumina nanofluid heat transfer in permeable medium influenced by Lorentz forces. Comput Methods Appl Mech Eng 349:839–858. https://doi.org/10.1016/J.CMA.2019.02.025

60. Singh RJ, Gohil TB (2019) The numerical analysis on the variation of electric potential, electric current and Lorentz force with its influence on buoyancy-driven conjugate heat transfer and fluid flow using OpenFOAM. Fusion Eng Des 148:111300. https://doi.org/10.1016/J.FUSENGDES.2019.111300

61. Soltanipour H (2020) Two-phase simulation of magnetic field effect on the ferrofluid forced convection in a pipe considering Brownian diffusion, thermophoresis, and magnetophoresis. Eur Phys J Plus 135:1–23. https://doi.org/https://doi.org/10.1140/epjp/s13360-020-00725-w

62. Ghofrani A, Dibaei MH, Hakim Sima A, Shafii MB (2013) Experimental investigation on laminar forced convection heat transfer of ferrofluids under an alternating magnetic field. Exp Therm Fluid Sci 49:193–200. https://doi.org/10.1016/J.EXPTHERMFLUSCI.2013.04.018

63. Yarahmadi M, Moazami Goudarzi H, Shafii MB (2015) Experimental investigation into laminar forced convective heat transfer of ferrofluids under constant and oscillating magnetic field with different magnetic field arrangements and oscillation modes. Exp Therm Fluid Sci 68:601–611. https://doi.org/10.1016/J.EXPTHERMFLUSCI.2015.07.002